LA-UR-14-22041
Approved for public release; distribution is unlimited.

Title: Evaluation of Deblur Methods for Radiography

Author(s): Wood, William M.

Intended for: Report

Issued: 2014-03-31 (rev.1)

LA - UR - 14 - 22041

# Evaluation of Deblur Methods for Radiography

Wm Monty Wood, P-23

## Introduction

Radiography is used as a primary diagnostic for dynamic experiments, providing time-resolved radiographic measurements of areal mass density along a line of sight through the experiment. It is well known that the finite spot extent of the radiographic source, as well as scattering, are sources of blurring of the radiographic images. This blurring interferes with quantitative measurement of the areal mass density. In order to improve the quantitative utility of this diagnostic, it is necessary to deblur or "restore" the radiographs to recover the "true" areal mass density from a radiographic transmission measurement.

Towards this end, I am evaluating three separate methods currently in use for deblurring radiographs. I begin by briefly describing the problems associated with image restoration, and outlining the three methods. Next, I illustrate how blurring affects the quantitative measurements using radiographs. I then present the results of the various deblur methods, evaluating each according to several criteria. After I have summarized the results of the evaluation, I give a detailed account of how the restoration process is actually implemented.

## Effects of Blurring on Quantitative Image Evaluation

To aid in the quantitative evaluation of radiographs, a "wedge" of known material thickness is typically included in every experiment, to provide an in situ "transfer function" as a scale to determine the areal mass density of the unknown, experimental object in the radiograph. The cross-section of such a transmission wedge is illustrated in Figure 1. (The dimension into and out of the paper is extended; hence, I label this the "prism wedge.") The most important aspect of this design is that opposing sides of the wedge have different slopes; i.e. the length scale over which the areal mass density changes is different for different sides of the prism. Using a synthetic radiograph of this type of prism wedge, one can see immediately the problem that blurring introduces into the quantitative analysis of the radiographs.

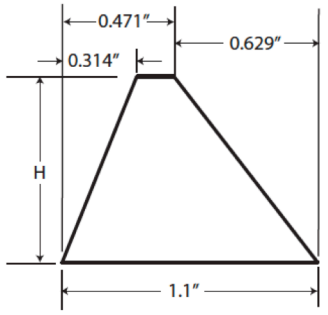


**Figure 1:** Design of "Prism" transmission wedge for in situ measurement of transfer function.

In Figure 2 I show the transmission "measured" from a synthetic radiograph of the prism wedge. The blurring of the synthetic radiograph was created to mimic the blur imposed in an actual radiograph. The differences in measured transmission between the "steep" and the "shallow" slopes for identical thickness of the wedge illustrate the fundamental problem which the blurring introduces into a radiographed image. *The measured transmission value of a feature depends fundamentally on the length scale associated with the feature.* In other words, the blurring of the image limits the utility of the radiograph as a quantitative tool in identifying the areal mass density associated with a given transmission. *In order to rectify this situation, it is necessary to "restore" or "deblur" the image data.*

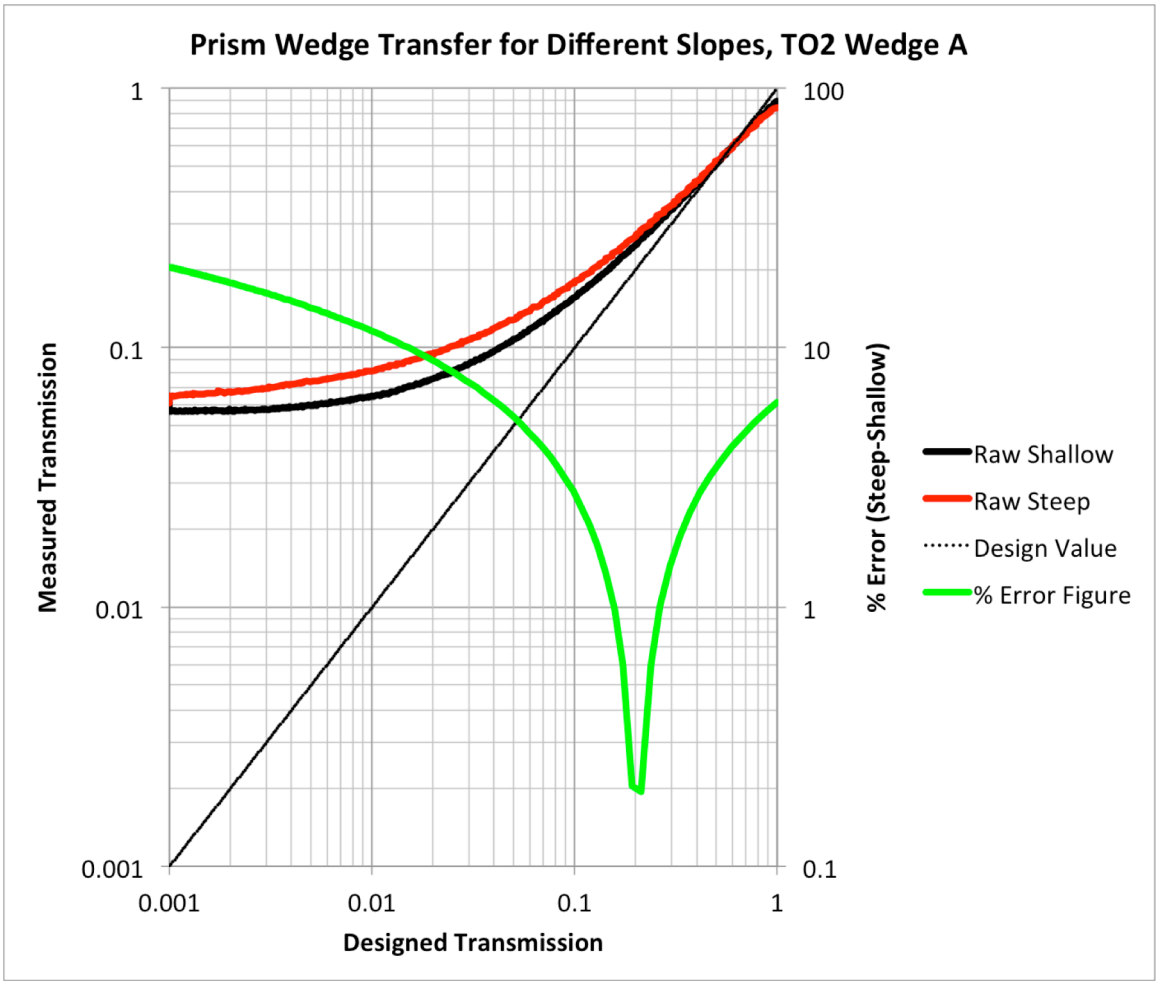


**Figure 2:** Comparison of measured transmission values through the Prism test wedge versus designed value for the two different slopes.

## The Deblur or "Restoration" Problem

The basic problem of deblurring can be demonstrated with the following equation[1]. If the image is denoted by *I*, the actual object denoted by *O*, the blurring Pont Spread Function or "PSF" denoted by *P*, and the noise in the measured image denoted by *N*:

$$I = O \otimes P + N \tag{1}$$

This describes the resulting image as the convolution of the object with the blurring function, with noise added. Written in this way, the problem assumes that the blurring within the image is *the same* at every point of the image. Mathematically, this quality is called "stationarity," and the process is referred to as a "stationary blurring" process. For the methods of deblurring evaluated herein, I am assuming a stationary blur process. It can be shown easily that the blurring of the radiographs is *not* stationary; however, it is worth seeing how well the assumption can help us.

In fourier space, the relationship between the fourier transforms of the various components is simpler:

$$\tilde{I} = \tilde{O} \bullet \tilde{P} + \tilde{N} \tag{2}$$

Here, the tilde over the letter indicates the fourier transform. Written in this way, the solution seems clear – simply divide the transform of the measured image by the transform of the PSF, and the resulting image will be the transform of the object. However, the noise term is the problem. Typical PSFs are peaked around low frequencies, and become very small at high frequencies. As a result, the fourier division results in a disproportionate enhancement of the high-frequency noise, and the result is, typically, unuseable. This is at the heart of the deblur problem: how to deblur an image to get useful results, while controlling the noise.

## Three Restoration Methods to be Evaluated

The three methods of deblurring which I will evaluate have all been used at some point in the standard suite of analysis tools. I will refer to them as follows:

FQ + δ: Fourier Quotient with Delta Noise Control

LFQ (for "Lutz Fourier Quotient"): Fourier Quotient with Frequency Cutoff

Tik: Fourier Quotient with Tikhonov Regularization[1]

The first of these, FQ, can be described with the following equation:

$$\tilde{O} = \frac{\tilde{I}}{\tilde{P} + k} \tag{3}$$

Here, $k$ is a constant, whose effect is to add a Dirac δ-function to the PSF. The noise is controlled by the magnitude of $k$. The division represents a point-by-point division of the 2D data in fourier space.

The second method, LFQ, uses a constant to control the noise in a slightly different way:

$$\tilde{O} = \frac{\tilde{I}}{\tilde{P}'(k)} \tag{4}$$

Here, the constant $k$ is used to make the frequency content by greater than (or less than) a fixed value:

$$\tilde{P}'_{\mathrm{Re}}(f) = \begin{Bmatrix} \tilde{P}_{\mathrm{Re}}(f) : \tilde{P}_{\mathrm{Re}}(f) > k \\ k \quad : 0 < \tilde{P}_{\mathrm{Re}}(f) < k \\ \tilde{P}_{\mathrm{Re}}(f) : \tilde{P}_{\mathrm{Re}}(f) < -k \\ -k \quad : 0 > \tilde{P}_{\mathrm{Re}}(f) > -k \end{Bmatrix} \tag{5}$$

Note that, in general, we are working with symmetric PSFs, so the transform is real. Essentially, the value of the transform is cut off at some minimum absolute value, while the positive/negative behaviour is preserved. Again, the magnitude of $k$ determine the amount of noise control.

Finally, the third method (Tik) is expressed in the following way:

$$\tilde{O} = \frac{\tilde{P}^* \tilde{I}}{\left|\tilde{P}\right|^2 + k\left|\tilde{H}\right|^2} \qquad (6)$$

In this expression, the $P^*$ represents complex conjugation, and the $H$ is a high-pass filter. As with the other expressions, $k$ expresses the noise control. (One can picture the effect of the high-pass in the denominator becomes, effectively, that of a low-pass in the overall equation.) Note, also, the similarity in appearance of this last expression to that of a Wiener filter.

## Requirements

In order to be considered as a candidate for deblurring data for quantitative evaluation, several requirements must be met. These are the following four items, and these are the four things which I will use to evaluate the methods.

### Consistency

When deblurring a scene, the values obtained for areal mass density after processing should be insensitive to the chosen noise control parameter, $k$.

### Noise Control

Obviously, the chosen method must enable control of the noise amplification inherent in the deblur process. In other words, the resulting, deblurred image must be useable.

### Edge Restoration

The deblurring method should be able to deblur the image of an edge, and result in a better Modulation Transfer Function.

### Accuracy

Finally, the image resulting from the deblur must represent accurately the actual data.

## Images for Use in Evaluation

For evaluating the first two requirements of Consistency and Noise Control, I will use the data from Gemini shots 1625-1631. These data include all the parts for the "standard analysis:" a flat field, a rolled edge, and the scene to be deblurred, which in this case is a Ta step wedge. Images of the step wedge (both synthetic and measured,) are shown in Figure 3. For the other two requirements, i.e. Edge Restoration and Accuracy, I will use two synthetic data images, Test Object 1 (TO1) and Test Object 2 (TO2,) illustrated in **Figure 4**. The square sections in the step wedge at top and bottom of TO1 have the same transmission values, but are arranged differently. These transmission values correspond roughly to those from the actual data Ta wedge. In addition, I have included a smaller step wedge which is placed at different positions within the image.

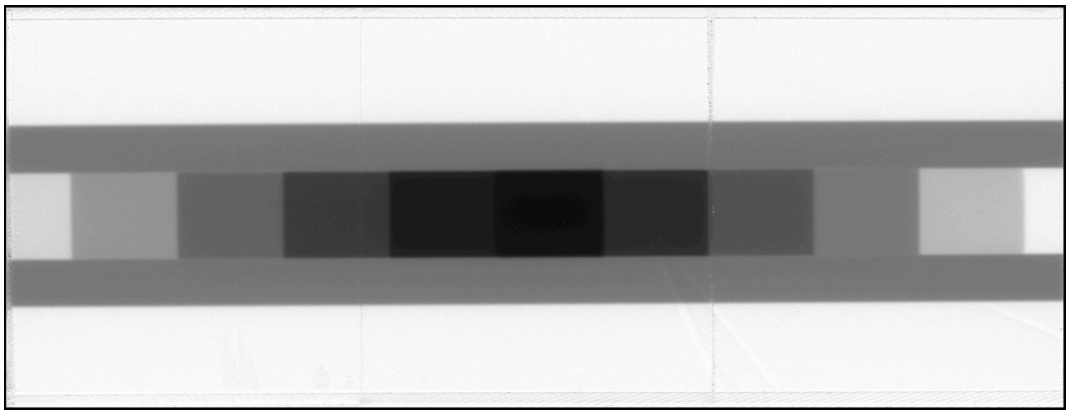

**Figure 3:** Measured radiograph of Ta step wedge, for evaluating deblur methods.

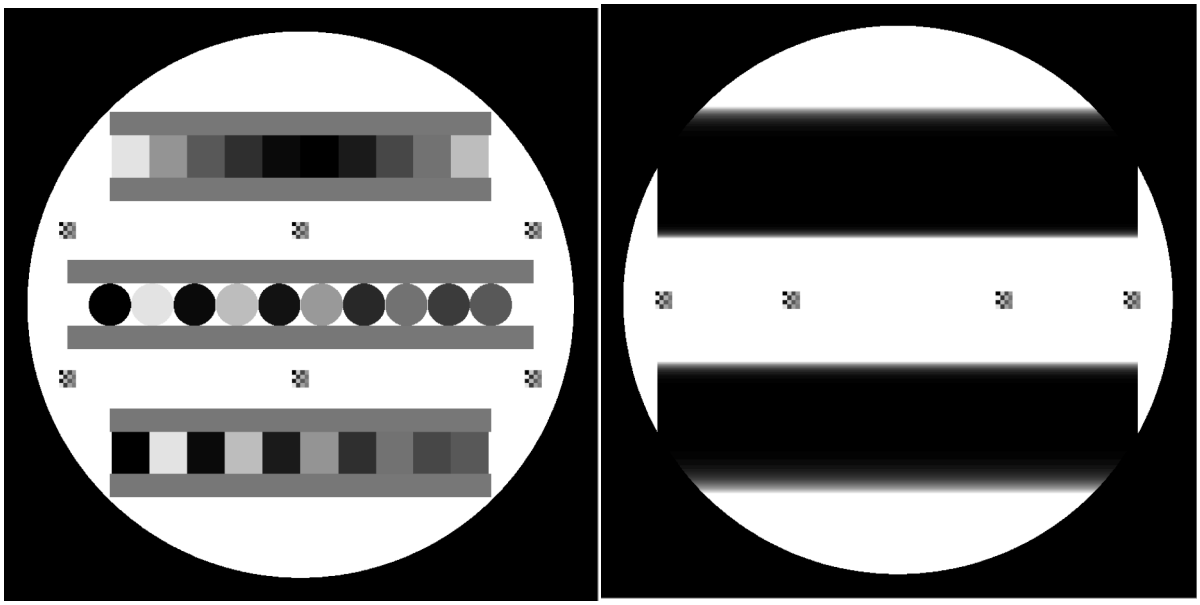

**Figure 4:** Synthetic Radiograph "Test Object 1" on the left, and "Test Object 2" on the right, not blurred, for evaluating deblur methods.

## Appearance of Restored Images

To give an idea of the appearance of the restored images, and how the noise control appears visually, I present a series of restored images. In **Figure 5** I show a section of the raw, blurred image, as well as three deblurs with low, medium, and high noise control, using the Tikhonov method. One can readily see the characteristic mottling associated with the deblur, as well as the "ringing" at the edges. In addition, it is clear that there is a trade-off between the "sharpness" of the image, and the amount of noise control. This type of appearance does not depend on method.

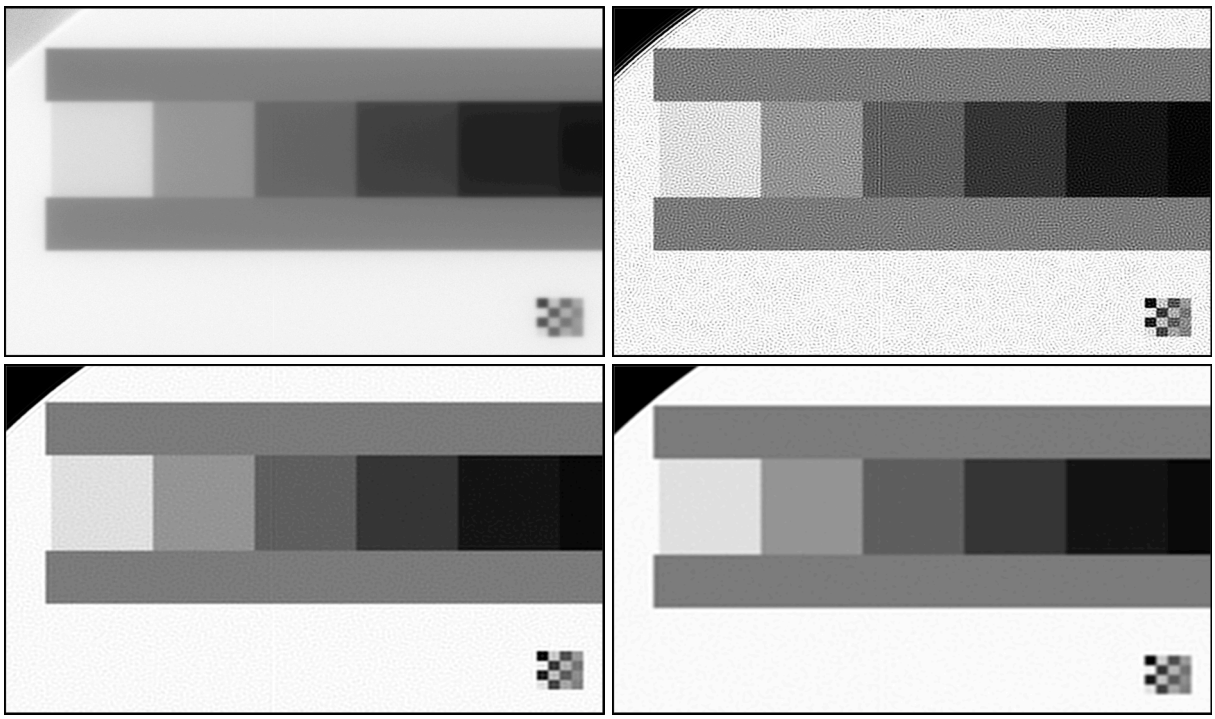

**Figure 5**: Various levels of noise control in deblurring using Tikhonov method. From left to right, and top to bottom, raw blurred image; deblurred image with low noise control; deblurred image with medium noise control; deblurred image with high noise control.

## Consistency

The first test for evaluating the restoration techniques is that of consistency. Using each restoration method, the image is restored, using several values for the noise control constant. The region where each step wedge segment shows within the image is defined, and the mean and variance of the pixel transmission values is measured in the region. This is done for wedge values "0" (outside the wedge) through "10," the thickest wedge segment. These values are then plotted to illustrate the consistency (or lack thereof) in the values obtained for each wedge segment transmission. Without any a priori knowledge of the transmission, these values *must* be consistent between deblurred images.

### FQ + δ

The first method, FQ+δ, yields the results shown in **Figure 6**. Because the addition of the δ-fn results in a change of the effective normalization of the PSF, the resulting restored image is multiplied by a constant to bring the value of the un-attenuated beam up to 1.0, or 100% transmission. This improves the results. In the "post-norm" results, the values from the raw data are also graphed. One can see readily the effects of the noise control; the variance of each step value diminishes as the noise is controlled. The variance of the step transmission values, *averaging across different noise control constants*, is larger than the variance of the measured raw step value variance, for the thicker wedge steps. This means that the deblur technique cannot produce consistent quantitative values in the deblurred images.

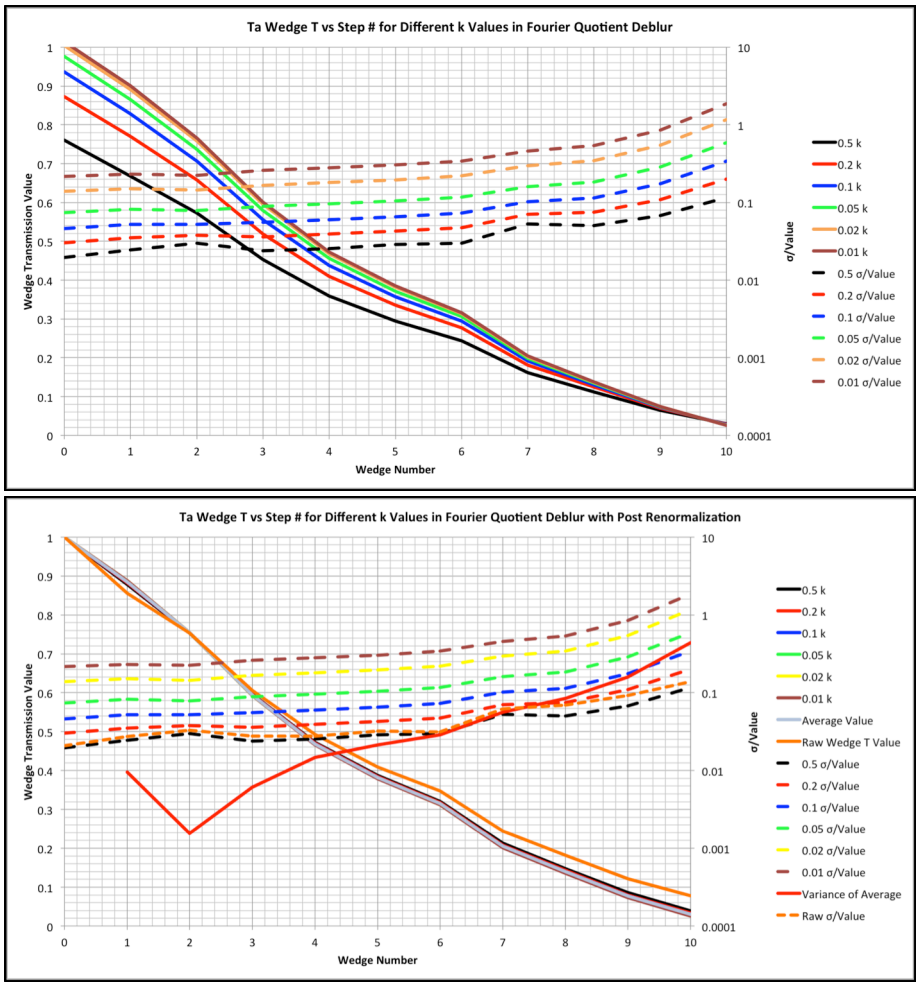


**Figure 6:** Comparison of wedge transmission values for FQ+δ restoration method. First graph shows values after direct deblur, with the variance associated with each value plotted along the log axis on the right. Bottom graph shows results after a "post-renormalization" procedure is applied, as well as the values obtained from the raw image with no processing. In addition, the variance across average step transmission values for different "k" (after the post renormalization) is shown.

## LFQ

The second method, LFQ, yields the results shown in **Figure 7**. For the same reasons as for the FQ+δ method, the resulting restored image is multiplied by a constant to bring the value of the un-attenuated beam up to 1.0, or 100% transmission. Again, this improves the results dramatically. As the noise control parameter is increased, the measured step value variance from the image decreases. Again, when the step transmission values are compared for many noise control values, the variance of this average cannot be made smaller than the measured variance from the image in the thicker steps. Again, this method does not pass the consistency test for quantitative image deblurring.

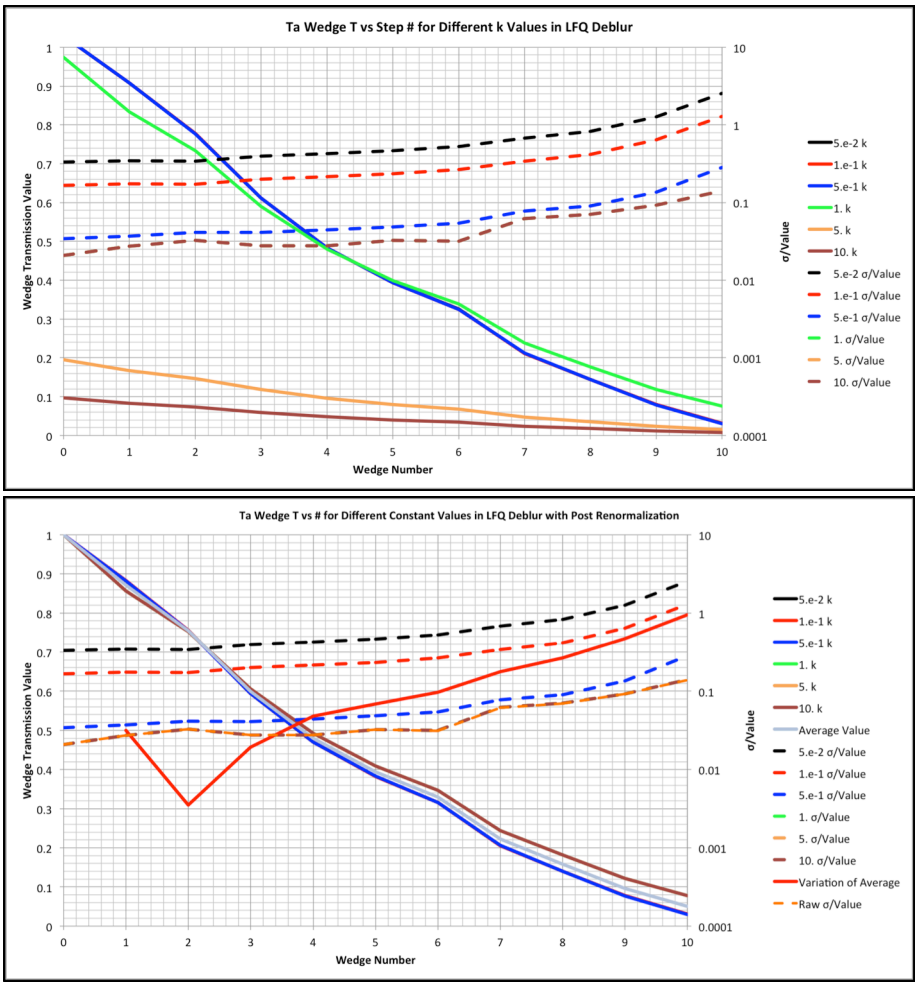


**Figure 7:** Comparison of wedge transmission values for LFQ restoration method. First graph shows values after direct deblur, with the variance associated with each value plotted along the log axis on the right. Bottom graph shows results after a "post-renormalization" procedure is applied. In addition, the variance of the average values for different "k" is shown.

## Tik

The final method, Tik, yields the results shown in **Figure 8**. Because both of the previous methods were subjected to a post-renormalization, the Tik results are, also. In this case, the improvement is minimal. The variation of the average values for different deblur constants is significantly less than the variance within each step, and is less than about 1%, except for the thickest step, which is 2%. This result does not change significantly for high pass filters of the form $(1 - (\text{Hamming Window})^N)$ across a wide range of "N" values. A visual demonstration of this consistent convergence is shown in **Figure 9**, where I plot overlaid lineouts through the TO1 step wedge for different values of the noise control parameter, *k*. The reduction in noise is clear, as well as the consistency of the average across the wedge step.

It is interesting to note, however, that when I use the "trivial" high-pass filter which is constant, i.e. it passes *all* frequencies, the results are almost identical to those found using LFQ; this is illustrated in **Figure 10**.

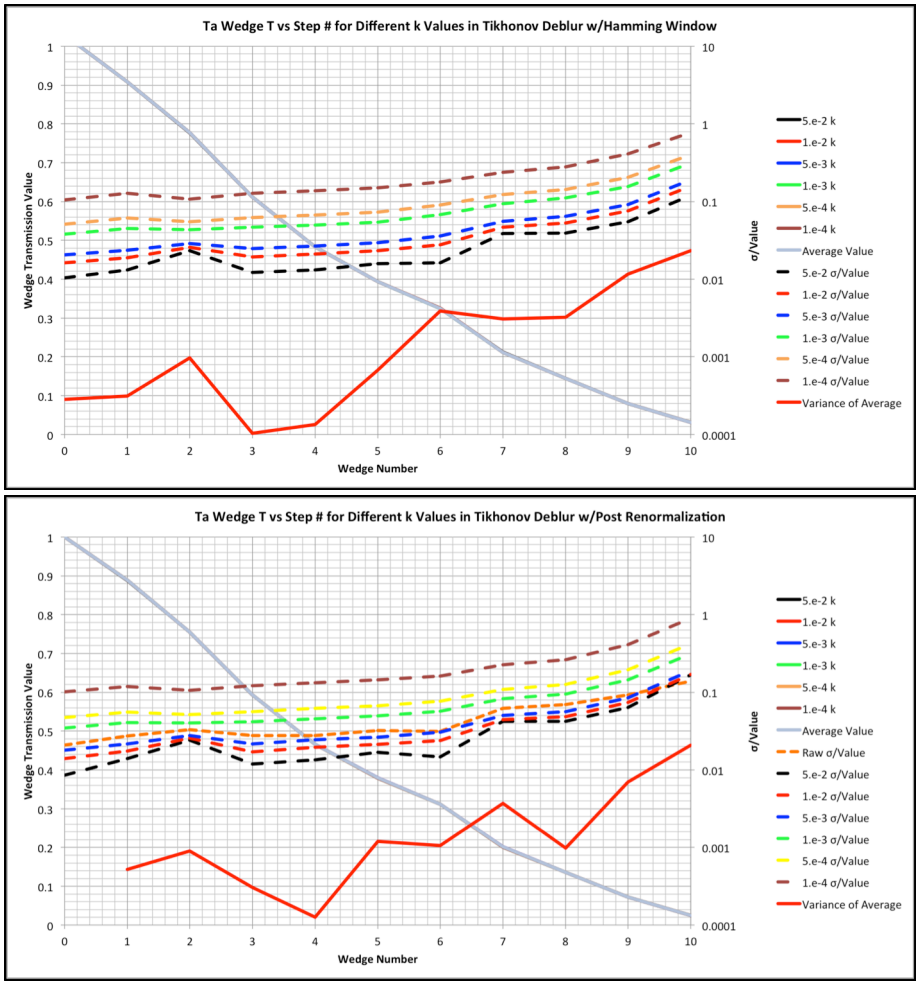


**Figure 8:** Comparison of wedge transmission values for Tik restoration method. First graph shows values after direct deblur, with the variance associated with each step value plotted along the log axis on the right. Bottom graph shows results after a "post-renormalization" procedure is applied. In addition, the variance of the average step transmission values for different "k" is shown.

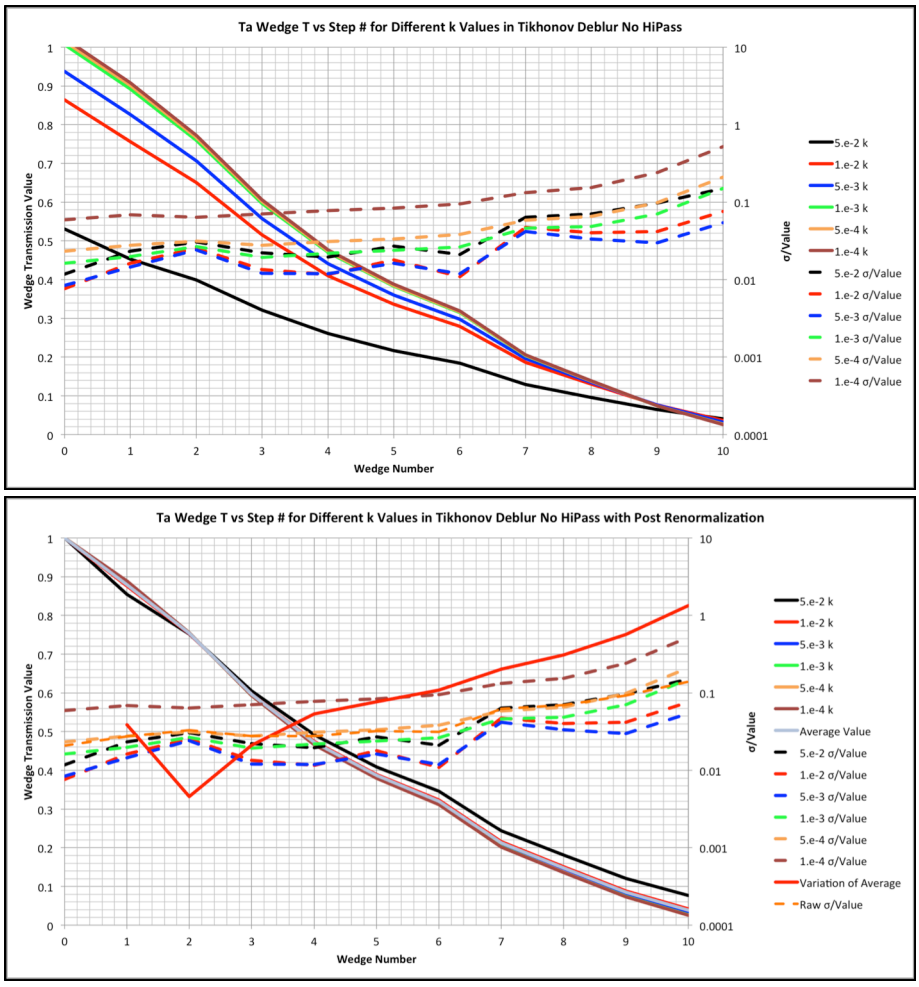


**Figure 10:** Comparison of wedge transmission values for Tik restoration method, using the "trivial" High Pass filter. First graph shows values after direct deblur, with the variance associated with each value plotted along the log axis on the right. Bottom graph shows results after a "post-renormalization" procedure is applied. In addition, the variance of the average values after the renormalization is shown.

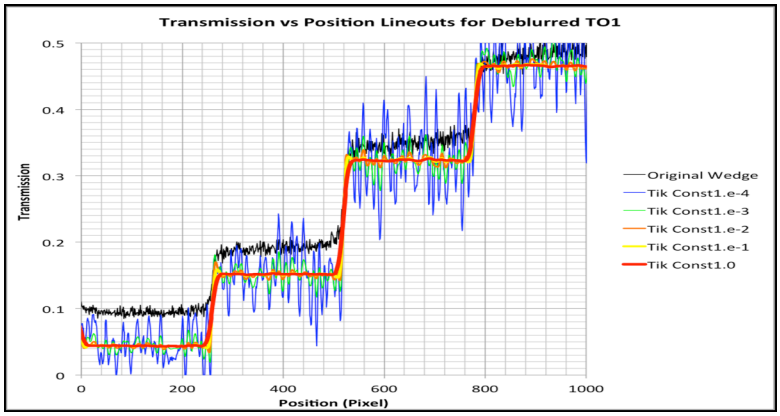


**Figure 9:** Lineouts of TO1 wedges for various values of noise control parameter in Tik Deblur.

# Noise Control

The second test of the quality of the restoration method is the control of the noise. Again, each method is evaluated below. I present, first, a few images that show the actual noise present in the images.

## Noise figure in the Images

In **Figure 11** I show the comparison between the frequency power spectra of a raw edge image, compared to a flat-fielded image. The raw image appears to display a significant amount of the frequency information associated with the actual edge. The flat-fielded data appears to have had much of this information "washed out" by the noise within the figure. Note particularly that in the direction along the edge, the power spectrum is significantly lower in the raw image, whereas the spectrum at high frequencies is commensurate in both directions for the flat-fielded image. This indicates that the actual noise spectrum is dominating at the higher frequencies (as one would expect.) In **Figure 12**, I show similar data for the synthetic edge

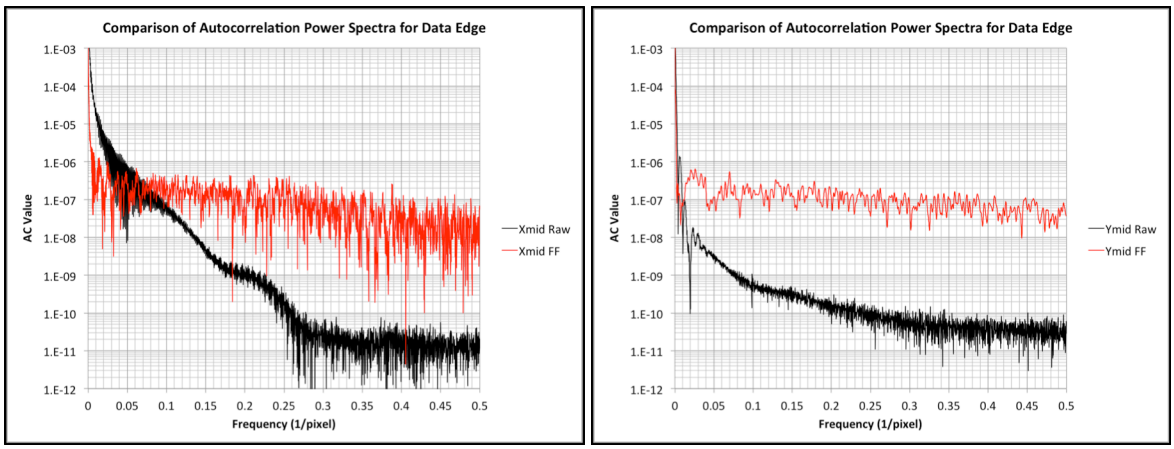


**Figure 11**: Comparison of autocorrelation line-outs for data image. Black curve is for the raw (de-starred and background subtracted) image; red curve is for the flat-fielded image. Left shows the frequency power spectrum "across" the edge; right shows the spectrum "along" the edge. Image power normalized to 1.0.

images. It appears that there is a more complex shifting of the energy through the frequency spectrum. In general, however, it still appears that in flat-fielding the image, (in this case going from the green curve to the red curve,) the noise figure dominates the power spectrum as one moves towards the higher frequencies. It also appears that my noise estimates are, perhaps, a bit conservative for the synthetic images.

These comparisons of the autocorrelations suggest that it might benefit the analysis if the detector response were measured with low noise in a different way than through a flat-field procedure, and thus reduce the noise introduced into the data. For example, it might be worth averaging a number of flat fields together, or perhaps measuring the detector/CCD system separately using different methods.

### FQ + δ

Referring again to **Figure 6**, the increasing value of the noise control constant does, indeed, reduce the value of the variance associated with each wedge step. However, even using a constant that begins to degrade the larger wedge step values (before renormalization,) the variance is significantly larger than that associated with the raw data. It is important to note that, within the raw data, the edges of the step region exhibit a significant curvature away from a constant value, so the comparison of the noise figure is actually, perhaps, worse than the graph indicates.

### LFQ

Referring to **Figure 7**, the noise control appears to be a little bit better than that that afforded by the first method. At the largest values of the noise control constant, i.e. those equal to 1.0 or above, the noise figure remains identical, and is actually the same as the raw data.

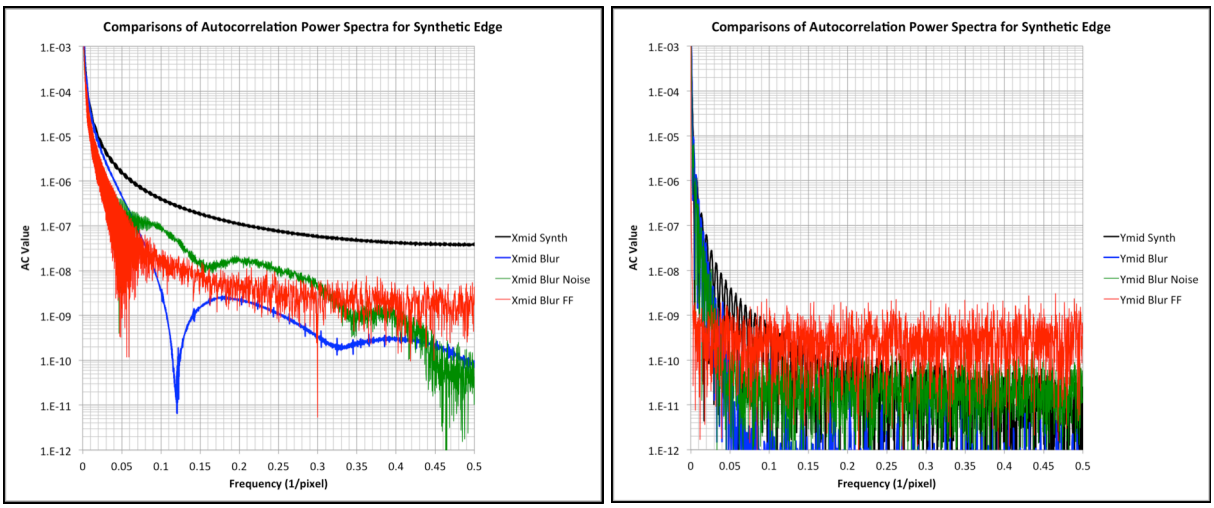


**Figure 12**: Comparison of autocorrelation line-outs for synthetic edge image. Black curve is for the simple edge; blue curve is for the blurred edge; green curve is the blurred and "detected" image with noise added; red shows the line-out for the flat-fielded image. Left shows the frequency power spectrum "across" the edge; right shows the spectrum "along" the edge. Image power normalized to 1.0.

### Tik

Looking again at **Figure 8**, it is seen that, using this method, the noise control is clearly much better than either of the other two methods. In addition, though not shown on the graph, further increase of the control constant brings the value of the variance down, without sacrificing the consistency of the wedge step value, up to a control constant value of 10 (this is as far as I have tested.)

# Edge Restoration

In order to evaluate the performance of the restoration techniques with a rolled edge, I consider both the actual data, and an ideal edge from the synthetic data. For both cases, I compare the actual lineout across the edge, as well as the MTFs for a series of deblurred images. In this section, all the techniques are presented overlaid upon each other.

## Data Edge Restoration: Shot 1629

Edges

In Figure 13, I show lineouts of restrored edge, using the various techniques outline above. It is clear that the edge itself is significantly sharper in each case, but there is also an overshoot on the high side, and an undershoot on the low side. The other oscillations are due to the left-over

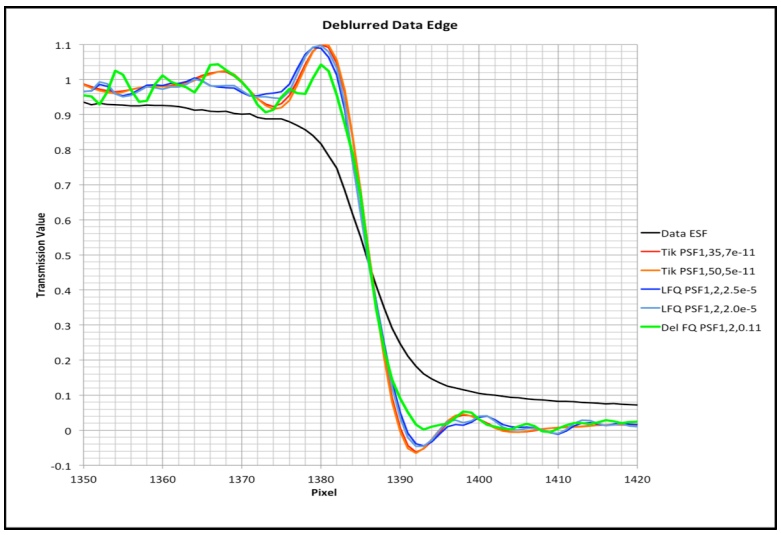


**Figure 13:** Reconstructed edges and original edge for different restoration techniques and noise control parameters.

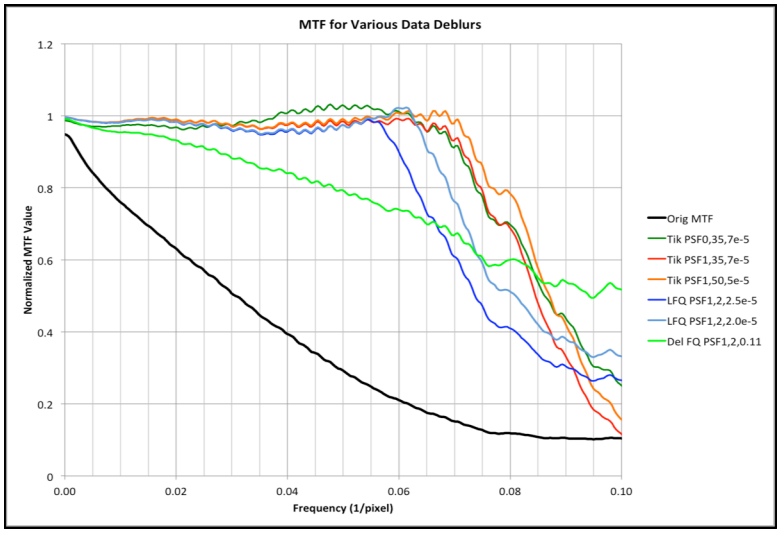


**Figure 14:** Modulation Transfer Functions from the edges reconstructed in Figure 13.

noise from the noise-control of the restoration. Part of this can be reduced by smoothing (which, in fact, makes the edge less steep,) but the overshoot problem remains.

Modulation Transfer Functions

In **Figure 14** I show the Modulation Transfer Functions, or MTFs, associated with the edges in Figure 13. Note that the edge which shows the least overshoot is that restored using the FQ + δ method, and this has apparently the worst MTF. The other edge restorations all have MTFs with a notable "corner" as they turn away from 1. Based on the standard interpretation of the MTF, the deblurred images display better resolution than the blurred image.

## Synthetic Edge Restoration: Hard Edges

Edges

Using an appropriate high-pass filter in the Tikhonov regularization, I see again the consistency; as the noise is controlled more, the value of the edge away from the transition

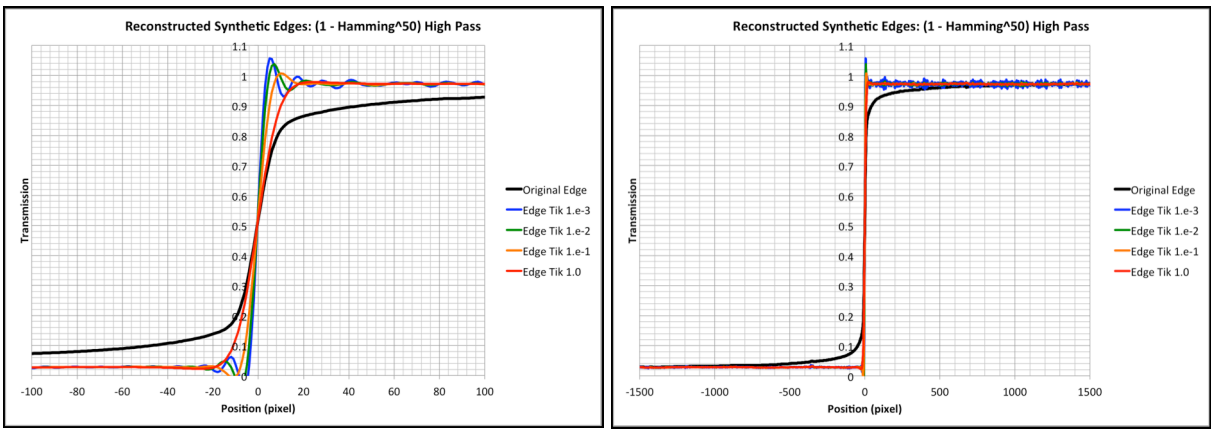


**Figure 15:** Reconstructed synthetic edges compared to the original, blurred, edge using a (1 – Hamming$^{50}$) high pass filter, for different noise control parameters.

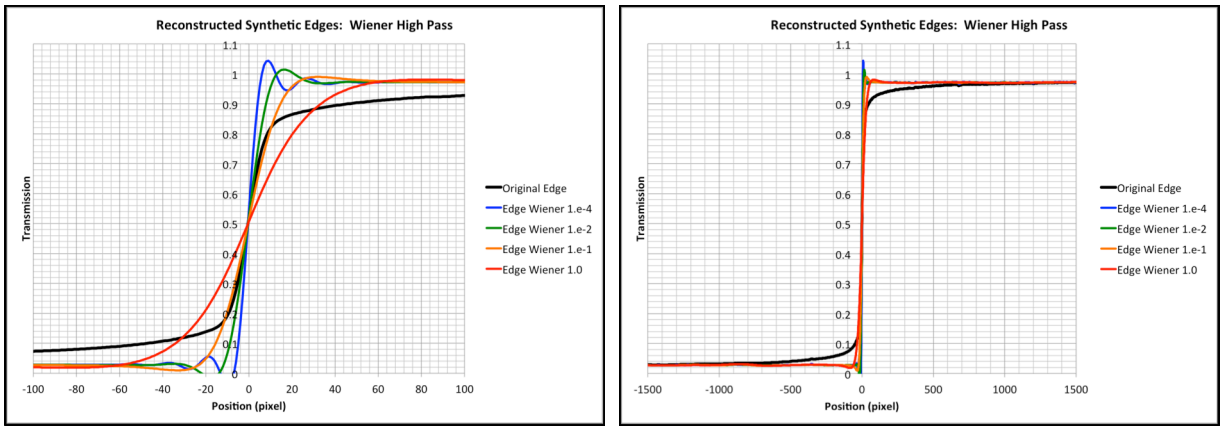


Figure 16: Reconstructed synthetic edges compared to the original, blurred, edge using a Wiener high pass filter, for different noise control parameters.

settles to a 'limiting' value, both at the transmissive side, and the non-transmissive side of the edge. To tie the choice of high pass to other, perhaps more familiar, methods, I have followed the condition described by a "Wiener" filter for one of the restorations.

In Figure 15 I show lineouts of the reconstructed, synthetic edge, for several noise control strengths, using a (1-Hamming$^{50}$) high pass filter. Note that, both on the transmissive, and on the obscured side, the transmission values have the same mean, and the variance depends on how tightly the noise is controlled. The high transmission is 0.972, and the low transmission is 0.028. The reason these are not 1.0 and 0.0, respectively, is that there is a "room glow" in the image, which is an additive constant background that is proportional to the total exposure of the scene. I will discuss this further in the next section.

In Figure 16 I show lineouts from a similar edge deblurring, using a Wiener filter with differing strengths of noise control. The actual edge slope in the restoration is higher using the Hamming window.

Modulation Transfer Functions

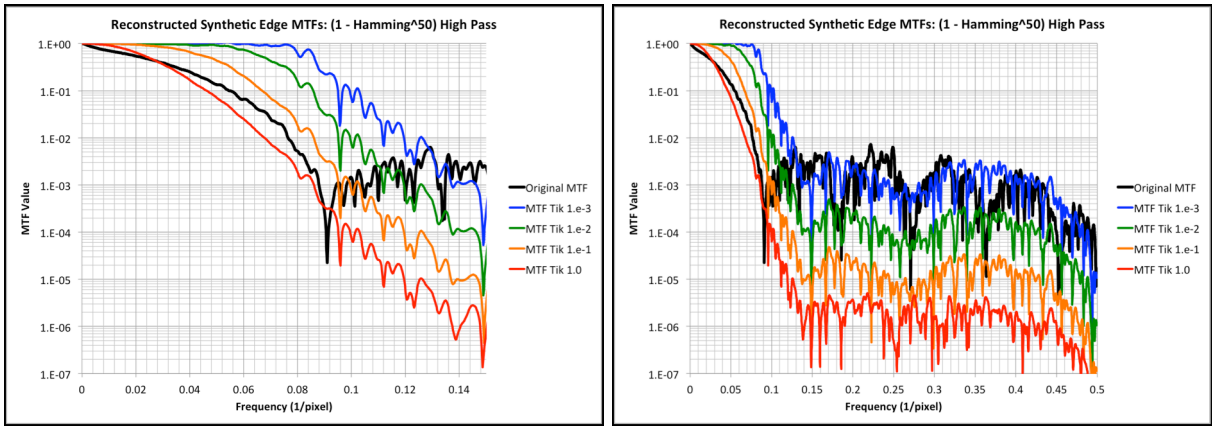


**Figure 17:** MTFs associated with the edge restoration above in **Figure 15**.

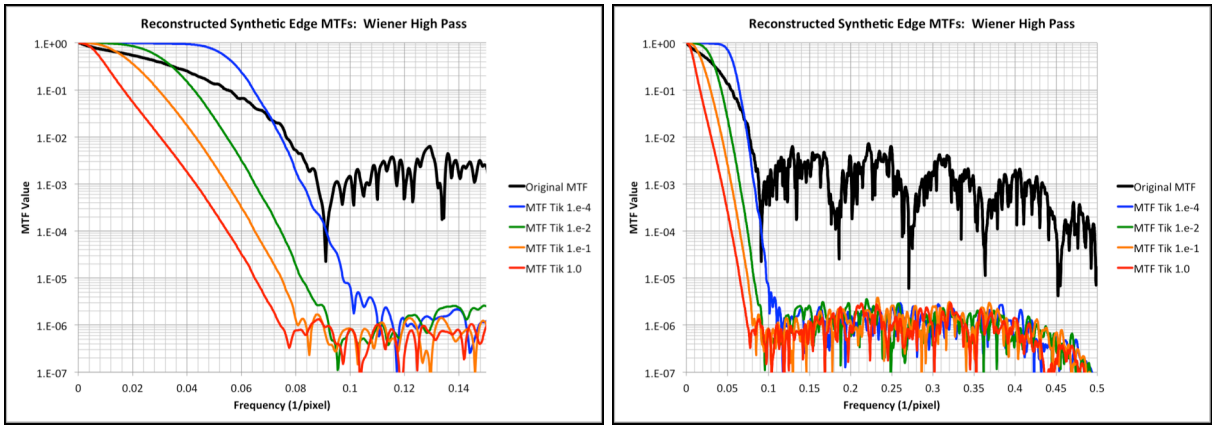


Figure 18: MTFs associated with the edge restoration above in Figure 16.

In Figure 17 and Figure 18 I show the MTFs associated with Figure 15 and Figure 16 . Note that, using the Hamming-type window, the MTF is near 1.0 out to a higher frequency. This is reflected in the better steepness of the reconstructed edges, as more frequencies are kept in the

deblurred image. One can see in the MTF of the original edge that the "noise figure" turns on at a frequency of about 0.09 /pixel. This represents visually the point where the spectrum of the noise overtakes the frequency spectrum of the signal of interest. It is this cross-over point which is used in defining the Wiener filter.

It should be noted that, using the Wiener filtration, one can actually extend the MTF significantly past the 0.09/pixel frequency. This comes, however, at the expense of significant noise in the image. *In evaluating images, this cross-over point is an indicator of the useful frequency content of an image.*

## Accuracy

In order to test the ultimate accuracy of the deblurring methods, it is necessary to create a synthetic blurred scene which captures the salient features of blurring of the actual data from a radiograph. Towards this end, I have created a set of "Test Objects," the details of which I describe in a separate document. Beginning with a scene of known transmission, the scene is blurred to accurately reflect the image formation process. Then, using the tools and methods which are used in actual data collection, i.e. measurement of a rolled edge in the object plane, as well as flat fields with nothing in the object plane, I deblur the resulting image, and compare the transmission values obtained to those in the un-blurred image. Note that, because both the (FQ + δ) and the LFQ methods do not display the necessary consistency to serve as candidates for restoration, I only describe the results for evaluation of the Tikhonov method.

Another issue which bears comment is that of "room glow," or a constant background due to, presumably, some scatter source. Evaluation of wedge transfer curves all show a need to have some background subtracted. Implicitly, I have assume that there is a constant background, and that this background is proportional to the total exposure of the scene. (This assumption of proportionality to the exposure recorded in the image is reasonable, since the collimation limits the exposure anywhere near the detection system to gamma rays that pass through the detector, or through the cone defined by the source and the illumination of the detector.)

### Test Object 1: Large Wedge

Using TO1, I explore the ability to obtain the original starting values of the step wedges, using the standard analysis techniques applied to the blurred and "noised" image. Wedge steps are approximately 250 x 250 pixels in the images.

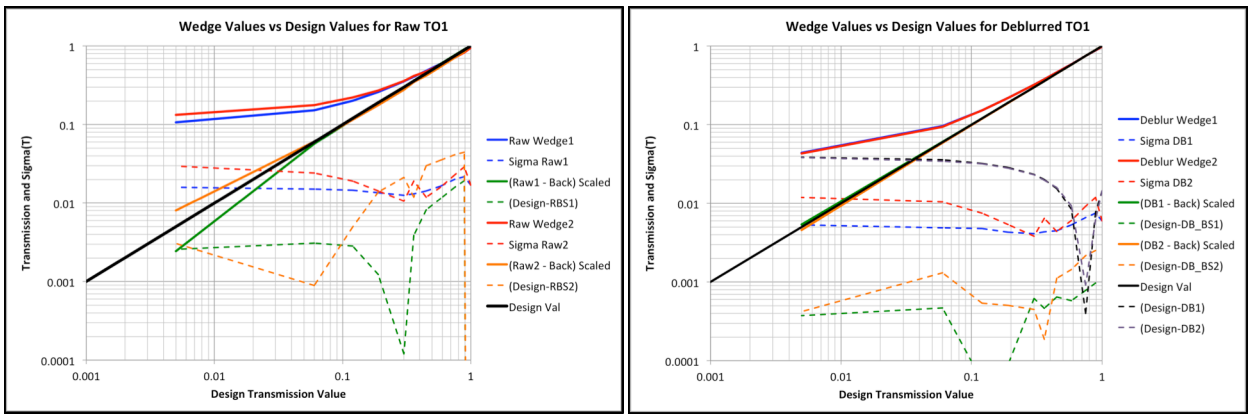


**Figure 19**: Plots of measured vs. design values for the two step wedges in TO1. Left plot shows the raw data in red and blue, with the variance in dotted. In addition, orange and green show the results for a constant subtracted off of image, with highest transmission normalized to 1.0. Right plot shows deblurred data, also with a background subtracted and high transmission scaled to 1.0. Difference from design value shown with orange and green dashed.

**Figure 19** shows the results of measuring wedge transmission values for the synthetic data. With the either image, it is possible to subtract a fixed background off, and scale the transmission where there is no material to 1.0. In the case of the raw, blurred data, the background level can be chosen so that the difference in the wedge transmission value from the original design value is within the measured variance of the data. It is clear, however, that both wedges cannot be well matched for a single value of the background.

When the data has been deblurred, the results are a little better than the raw. However, when the fixed background and the scaling are applied, the results are significantly better. Besides being significantly closer to the design values than the inherent variance across the wedge, the difference from the design value is less than 1% of the actual value for most of the wedges, with the exception of the thickest part, where the error is about 8%, and one of the middle wedges (T=0.06, with measured error of 2.5% of this.)

At this point, the subtraction of the fixed background begs the question, "How do we determine the fixed background?" I will discuss below a method for estimating the fixed background, which I am calling "room glow." To illustrate how this room glow value will be

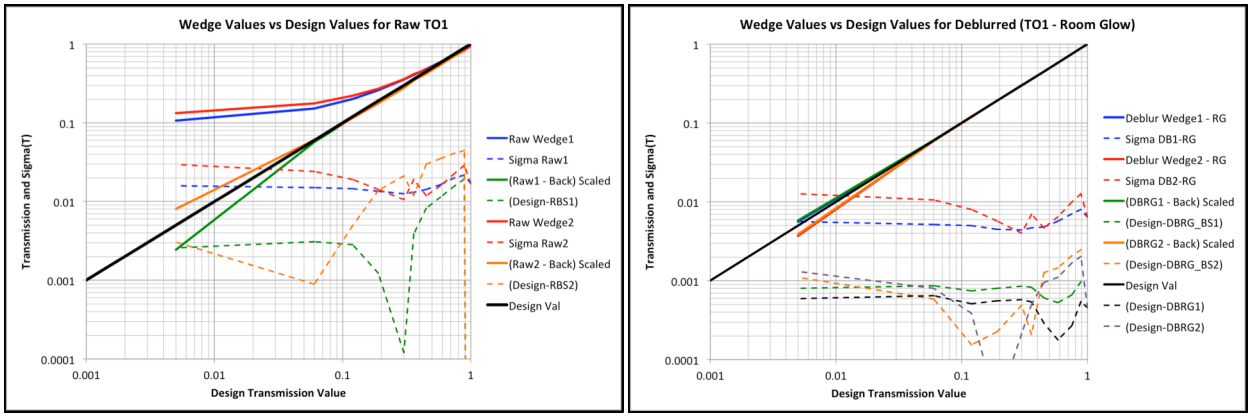


**Figure 20**: Plots of measured vs. design values for the two step wedges in TO1. Left plot shows the raw data in red and blue, with the variance in dotted. In addition, orange and green show the results for a constant subtracted off of image, with highest transmission normalized to 1.0. Right plot shows deblurred data, also with a background subtracted and high transmission scaled to 1.0. Difference from design value shown with orange and green dashed.

used, I present **Figure 20** which shows the same results as the previous figure, with the difference that the right hand figure shows the results of subtracting off the "known" room glow value from the images as part of the processing. On can see that the difference between the averaged value and the design value is smaller by an order of magnitude than the sigma of the averaged wedge value ( obviously, this sigma can be reduced by more noise control, at the expense of the sharpness of the edges.) For comparison's sake, I also compare the result of subtracting off a uniform background and scaling; the results are actually worse than the image straight from the deblurring. The greater error at the low transmission end is due to the larger relative noise, coupled with the fact that the image only contains positive values.

### Test Object 1: Small Wedge

I can investigate the same set of criteria for accuracy, using the small step wedges in the images. Steps here are approximately 30x30 pixels. With the smaller length scales involved, there is more of an effect of the limits on the useable bandwidth of the restored images.

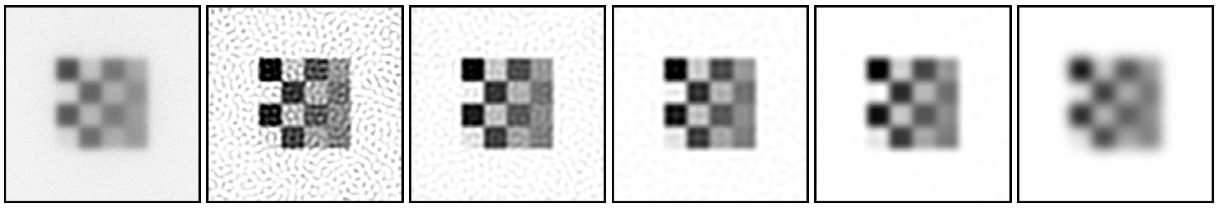

**Figure 22:** Images of small wedge, starting with the raw, flat-fielded image on the left, and proceeding through deblurs using increasing noise control going from left to right.

In **Figure 22** I show a series of images of one of the small step wedges from TO1. The original blurring can be seen in the left image. Following this, there is a series of images starting with little noise control, with increasing noise control as the images go from left to right. Here is seen again the trade-off between the degree of the noise control, and the sharpness of the edge.

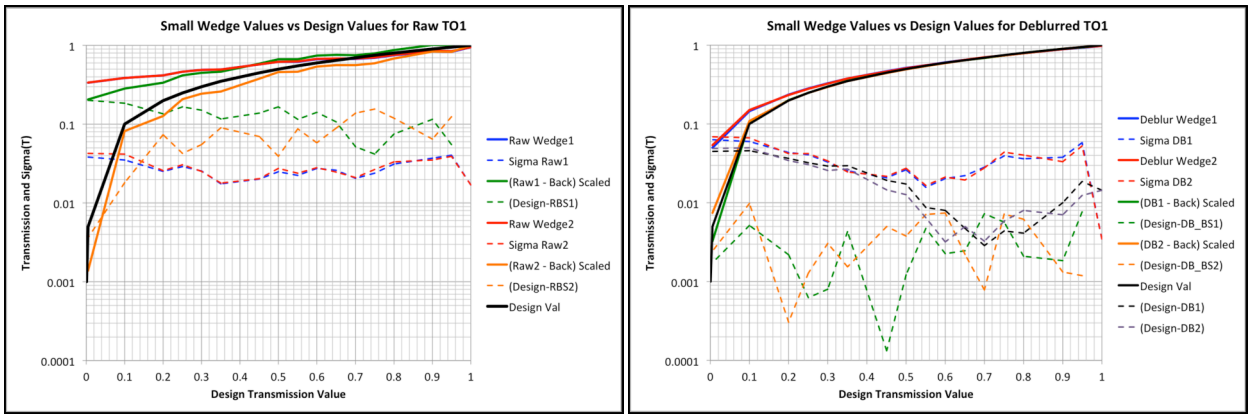


**Figure 21**: Plots of measured vs. design values for two of the small step wedges in TO1. Left plot shows the raw data in red and blue, with the variance in dotted. In addition, orange and green show the results for a constant subtracted off of image, with highest transmission normalized to 1.0. Right plot shows deblurred data, also with a background subtracted and high transmission scaled to 1.0. Difference from design value shown with orange and green dashed.

Also, at these smaller length scales, the noise plays a large role within the interior of the wedge steps. When the noise figure appears to be well-controlled, the edge seems nearly as blurred as the original image.

In **Figure 21** and **Figure 23** I show the results corresponding to the comparisons of the larger wedges above, for measurement of the small wedges. Wedge 1 is located near the center of the image. Wedge 2 is located near the edge of the collimation. With the raw data, the mismatch of the measured compared to the design value is significantly worse than was observed for the large wedges. Even when a background is subtracted and the 100% transmission is scaled, it is impossible even to match one wedge accurately, much less both at the same time. The difference between the design and measured values is larger than the sigma associated with the wedge value measurement. On the right of **Figure 21**, I graph the results of measurement after deblurring. For this case, the difference between measured and design value is right about equal to the sigma of the measurement. When the uniform background and scaling are applied, the results become significantly better.

In **Figure 23** I show the same results, but now the deblur process in the right side graph has been applied to the images with the room glow subtracted. As above with the larger wedges, the

measured values of the deblurred wedges are significantly closer to the design values than the sigma of the measurements. In addition, with a background subtract and scaling, some wedge values improve, while others get worse; overall, the result of subtraction and scaling seems not to improve these results significantly.

It should be noted that appears to be a slightly greater discrepancy between the two wedges, which I am inclined to ascribe to the fact that one is significantly closer to the collimation of the image. That being said, I would still claim that the deblurred results are still acceptable, given the constraints imposed by the presence of noise in the detection system.

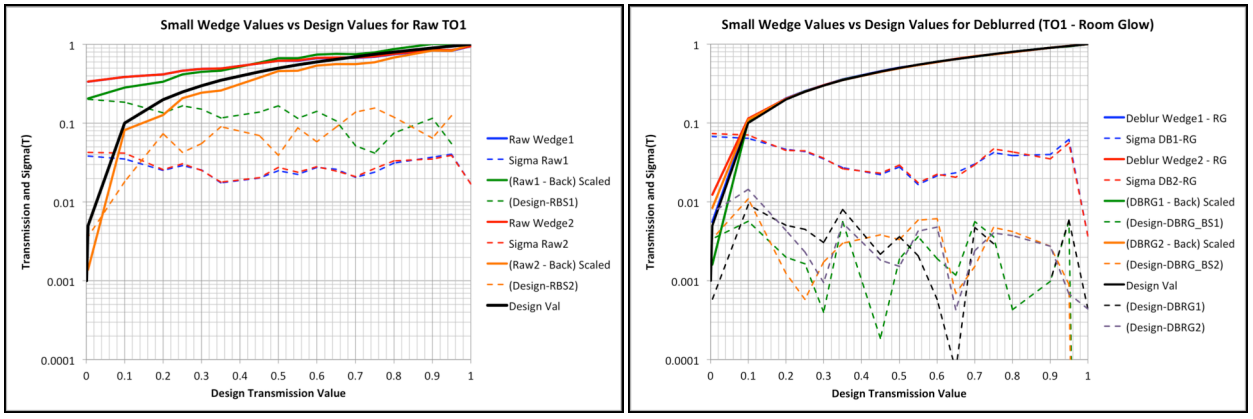


**Figure 23**: Plots of measured vs. design values for two of the small step wedges in TO1. Left plot shows the raw data in red and blue, with the variance in dotted. In addition, orange and green show the results for a constant subtracted off of image, with highest transmission normalized to 1.0. Right plot shows deblurred data with the room glow subtracted, also with a background subtracted and high transmission scaled to 1.0. Difference from design value shown with orange and green dashed.

## Test Object 2: Prism Wedges

The prism wedges can be studied in much the same way as the step wedges. I show the transmission plots of lineouts for the raw and deblurred TO2 in **Figure 24**. As expected, the deblurred images can be matched well by subtracting a uniform background, and scaling the

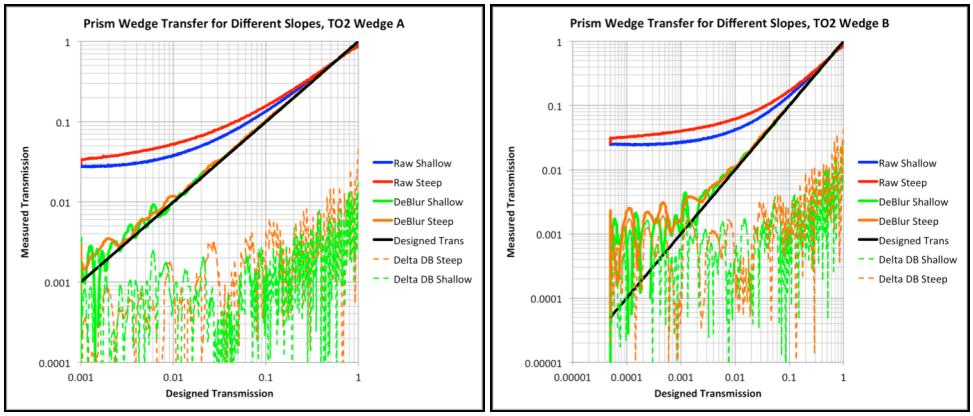


**Figure 24**: Plots of measured vs. design values for lineouts of the two wedges in TO2, comparing raw with the deblur of the room glow corrected images.

100% transmission to 1.0. The accuracy of the restored image compared to the designed value is around 1% of the transmission value near the thin part of the wedge, but this slowly gets larger, until the signal-to-noise is equal to 1, right about 0.001 transmission, and the delta between measured value vs. design value begins to intersect the design value. This is a nice illustration of the signal-to-noise reducing to 1 at low transmission parts of the image. Note, also, that at the low transmission values, the curves from the deblurred wedges show transmission higher than the design value. This is a result of the fact that the detection system does not allow negative values, so we are, in some sense, folding the noise distribution over on itself near zero transmission.

As with the step wedges, the restoration of the prism wedges displays the same consistency of average value. At the transition from wedge to no wedge, there are varying degrees of

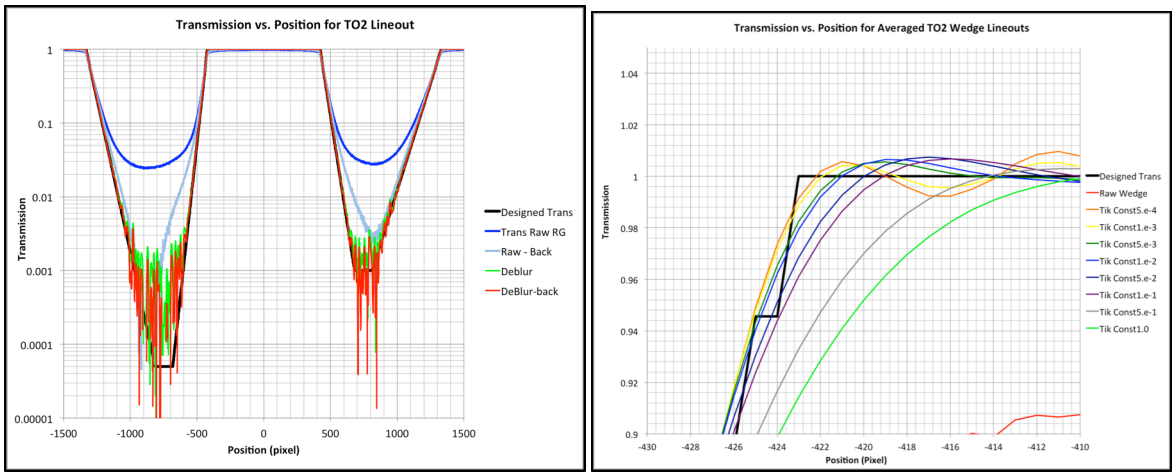


**Figure 25**: Plots lineouts vs. position for the TO2. Graph on left shows lineout of an averaged set of lines through both prism wedges. Right graphs shows the thinnest part of the steepest edge of the deeper prism, as it transitions to no wedge.

overshoot. The positive nature of the images is shown in the lineout in **Figure 25**. The noise of the deblurred image "kisses" the design value, but a slight background subtraction is needed to make the average value equal the design value. At the transition, the degree of overshoot is seen to change as the noise control parameter is varied. For this illustration, the restoration associated with the 0.01 constant shows less than a 1% overshoot, with about 9 pixels after the transition before the overshoot settles back to the 100% transmission level (1.0.) This sits well with the MTF graphs above, where the highest "useable" frequency was around 0.1 / pixel. This inverts to 10 pixels. Again, as with the hard edge, the overshoot seems to be systematic, and suggests that there may be a straightforward way to handle within images.

**Presence of "Room glow"**

As indicated above, there is evidence that, to first order, our images have a uniform background that is proportional to the total exposure of the image. This background I have labeled "room glow," implicitly assuming that its origin is scattering of the beam from whatever is in the path of the beam. (These experiments typically where performed with the "get lost" hole in the camera box covered with a plate, e.g.) In order to determine the proportionality constant, it is simply necessary to observe the values obtained when deblurring the rolled edge. Because the edge image has very close to one half the exposure of the flat field image, the dark side of the edge will deblur to the background value associated with the edge, and the bright side will deblur to 1.0 plus the edge background value, - the flat field value, which should be *twice*

that of the edge image. In other words, the bright side of the edge will be as much less than 1.0 as the dark side is greater than 0.0. Clearly, adjustments in the actual data must be made to accommodate shot-to-shot variations in beam dose.

## Summary of Evaluation Results

To begin with, the use of Tikhonov regularization in the one-step deblur or "restoration" process is clearly the best of the three methods outlined above, based on the consistency of deblur values of step wedges as the noise control parameter is varied. In addition, it is possible to control the noise so that the sigma associated with the deblurred image is comparable to, or smaller than, that associated with the raw data within a single step, while still improving accuracy of the measured value of the wedge. This fact is true down to transmission levels where the signal-to-noise level is less than 1. The only part of the images where greater care must be taken is in the presence of "edges," i.e. discontinuities in the second spatial derivative of the transmission value. One can think of this as related to a spatial resolution issue – i.e. the "overshoot" associated with the edge restoration limits the accuracy as one gets closer to the edge.

## Continuing Research: Issues to be Addressed

The primary issue of obvious concern is the overshoot at edges and discontinuities of the gradient in the restored images. For a region that changes from one gradient to another suddenly (i.e. an effective δ-function second derivative,) the overshoot under reconstruction appears repeatable and predictable, even though the restoration may not look satisfying. To quantify this statement, though, a more thorough investigation of the reconstruction of edges, and transmission gradients, is warranted. It should be noted that, as the noise is controlled with more strength, the overshoot diminishes, as well as the steepness of the reconstructed edge, and the length scale over which the change in transmission slopes is fitted gets larger. This points towards some sort of limiting procedure which could be applied to the problem, and which I will explore in a separate paper.

## Conclusions

The single step restoration process, described by equation (6), shows clear advantages over the other two methods which have been used as part of the standard data analysis suite for radiographs. In the case of step wedges, the technique is more than adequate to provide the accuracy desired as part of the experiment. Further improvements will entail improvements to the actual data collection hardware. Because of the systematic nature of the overshoot of edges under restoration, it should be possible to improve the quality of hits aspect of the deblurring process as well. This will be the topic of a second paper.

## References

1) Jansson, P.A., Deconvolution of Images and Spectra, 2nd Edition, Academic Press, San Diego 1997.

## Appendix: Details of Restoration Implementation

Below I outline the step-by-step process for processing the radiographic image data. In what follows, $I_{raw}$ refers to the raw data image, $F$ is the flat field, $E$ is the edge image, $P$ is the PSF image, $I_{proc}$ is the processed image, M is the mask which follows the collimation in the image, and $O$ is the "actual" image of the object.

**Subtraction of Dark Field**

Along with each shot, a "darkfield" is taken, which is a data read of the CCD detector, with no x-rays applied to the system. This image is subtracted off of the data image:

$$I_{proc\_DF} = I_{raw} - I_{DF}$$
$$E_{proc\_DF} = E_{raw} - E_{DF}$$
$$F_{proc\_DF} = F_{raw} - F_{DF}$$

**Destarring of Images**

X-ray photons that strike the CCD array directly can cause pixels to saturate, giving the appearance of "salt-and-pepper" in the image. The effect of this is removed prior to further processing using a median filter. At each point, a neighborhood around the point is compared. If the value at the point is outside of several standard deviations of the average, the value of the point is assigned to the median of the neighborhood. Several passes of this process appear to be effective at removing the stars in each of the images:

$$I_{proc\_DS} = Destar(I_{proc\_DF})$$

**Correction of Tile Glow**

The crystal detector which converts x-rays to visible light is pieced together, and there is a "glow" associated with visible light scattering within each separate panel of the detector. This "tile glow" is approximately proportional to the total signal within the tile. This signal removal is applied to each image.

$$I_{proc\_TG} = \sum_{n} (I_{proc\_DF\_Tn} - k_T \int I_{proc\_DF\_Tn})$$

**Subtraction of Room Glow**

In a way similar to the tile glow removal, the room glow is removed in each image:

$$I_{proc\_RG} = (I_{proc\_TG} - k_R \int I_{proc\_TG})$$

**Flat Fielding of Images**

At this point, the detection spatial dependence, as well as beam profile, is removed by dividing by the flat field image in a pixel-by-pixel fashion. The flat field image is constrained so that no pixel value is less than 1:

$$I_{proc\_FF} = \frac{I_{proc\_RG}}{\left(F_{proc\_RG} > 1.0\right)}$$

**Determination of PSF from Edge Image**

With this step, the edge image is used to determine a line spread function, or LSF, by taking the derivative across the edge. A subtle point here is to recognize that the *image* of the edge is not an *infinite* edge. The process of going from LSF to PSF via derivative of the edge implicitly assumes an infinite edge. To account for this, a synthetic edge is forward blurred with the PSF, the synthetic ESF compared to the data, and adjustment are made as needed to get a better PSF. Several iterations usually will do the trick.

Because of the noise in the image, several rows of the edge image are averaged, and a functional fit is applied to the edge, which allows for a smooth derivative. The fit used assumes a symmetric LSF. This LSF is then Abel inverted to give the PSF. The image of the PSF is then made from this PSF by assuming axial symmetry, and creating an image of PSF($r$). Implicit in this procedure is the assumption that the blurring of an *object* radiograph is the same as the blurring of an *edge*:

$$Edge = Average(E_{proc\_FF})$$

$$LSF = \frac{d(Edge)}{dx}$$

$$PSF = Abel^{-1}(LSF)$$

$$P = PSF(r)$$

I have found that, for the edges that are typically measured, a functional form that works well is:

$$Edge(x) = \frac{a_1}{2}\left[1 + erf\left\{a_2(x-\mu)\right\}\right]$$
$$+a_3\left\{\frac{1}{\pi}ATAN\left[a_4(x-\mu)\right]+\frac{1}{2}\right\}$$
$$+a_5\left\{\frac{1}{\pi}ATAN\left[a_6(x-\mu)\right]+\frac{1}{2}\right\}$$
$$+a_7\left\{\frac{1}{\pi}ATAN\left[a_8(x-\mu)\right]+\frac{1}{2}\right\}$$

$$LSF(x) = \frac{a_1 a_2}{\sqrt{\pi}}e^{-a_2^2x^2} + \frac{a_3 a_4}{\pi\left[1+a_4^2x^2\right]} + \frac{a_5 a_6}{\pi\left[1+a_6^2x^2\right]} + \frac{a_7 a_8}{\pi\left[1+a_8^2x^2\right]}$$

$$PSF(r) = \frac{a_1 a_2^2}{\pi}e^{-a_2^2r^2} + \frac{a_3 a_4^2}{2\pi\left[1+a_4^2r^2\right]^{3/2}} + \frac{a_5 a_6^2}{2\pi\left[1+a_6^2r^2\right]^{3/2}} + \frac{a_7 a_8^2}{2\pi\left[1+a_8^2r^2\right]^{3/2}}$$

Note that, in keeping the analytic forms, computer time is minimized, and the Abel inversion process does not give the "limning" at large *r* because of the implicit truncation of the LSF due to a finite data set.

**Restoration of Image**

Finally, with the PSF in hand, I can perform the restoration of the image. To begin with, the "convexity" across the image associated with the blurring of the flat field has been removed by division of the flat field. This convexity is replaced by forward blurring a synthetic flat field, and multiplying the flat fielded image by this. Second, the blur information outside of the collimation is, simply put, not there. To approximate this information, the image is masked at the collimation boundary, and forward blurred using the PSF. The blurred image outside the mask is then pasted to the processed image, and the deblur proceeds:

$$\tilde{F}_{SynthBlur} = \tilde{M} \bullet \tilde{P}$$

$$I_{proc\_Final} = I_{proc\_FF} \bullet F_{SynthBlur}$$

$$\tilde{I}_{proc\_Blur} = \tilde{I}_{proc\_Final} \bullet \tilde{P}$$

$$I_{ToDeblur} = \left[I_{proc\_Final}\right]_{InsideMask} + \left[I_{proc\_Blur}\right]_{OutsideMask}$$

$$\tilde{O} = \frac{\tilde{P}^*\tilde{I}_{ToDeblur}}{\tilde{P}^*\tilde{P} + k\left|\tilde{H}\right|^2}$$